



Numerical and experimental analysis of elastic–plastic pure bending and springback of beams of asymmetric cross-sections



M. Sitar, F. Kosel, M. Brojan*

Laboratory for Nonlinear Mechanics, Faculty of Mechanical Engineering, University of Ljubljana, Askerceva 6, SI-1000 Ljubljana, Slovenia

ARTICLE INFO

Article history:

Received 24 July 2014

Received in revised form

21 October 2014

Accepted 1 November 2014

Available online 7 November 2014

Keywords:

Elastic–plastic bending

Asymmetric cross-section

Springback

Elastic modulus evolution

Experiments

ABSTRACT

We present a procedure for numerical computation of elastic–plastic bending and springback of beams with asymmetric cross-sections. Elastic–nonlinear hardening behavior of the material is assumed and both isotropic and kinematic hardening models are considered. The strains are described as a function of rotation and shift of the neutral axis and the curvature of the beam. Exact geometric expressions for large deflections and large rotations are taken into account during bending process. A complete loading history is taken into account including the effect of the local loading during the monotonic decrease of the load. Numerical examples confirm a strong influence of the load on the final and springback rotation of the neutral axis, its shift, and curvature of the beam for different cross-sections and materials. A custom made forming tool was designed and manufactured in-house to experimentally evaluate the proposed solution procedure. It is shown that relative difference between experimentally and theoretically predicted results of the final radius of curvature of the formed beam is $0.177 \pm 0.683\%$, if also the effect of pre-strain on elastic modulus is taken into consideration.

© 2014 Published by Elsevier Ltd.

1. Introduction

Either as vital parts of load-bearing structures in mechanical and civil engineering or merely as an aesthetic feature in architecture, curved beams are most commonly made via some sort of forming process. V-bending, roll-bending, air and edge-bending, hydroforming, etc. are some of the examples of technological/manufacturing processes for obtaining the desired shape. The prediction of the (final) shape can be a complex task, especially because real-life materials often exhibit nonlinear mechanical response to loading.

In the forming process, the material undergoes elastic–plastic deformations. The plastic part of deformation changes the original shape of the object permanently, whereas the elastic part returns the deformed shape back towards initial configuration. Since a certain amount of elastic deformation is practically always present, the final shape of the object is not the same as the shape of the forming tool itself. A common way to deal with this problem is to add special techniques to reduce the effect of elastic recovery (also known as springback), such as extra features in radii, using smaller radii, or varying blankholder force in the forming process. These techniques reduce the effect of springback, but the formed part will always tend to springback by a certain amount.

In the available literature one can find a considerable number of papers devoted to this subject. Kosel et al. [1] presented an analytical solution of the simplified model for predicting the springback of beams made from material with an elastic–linear hardening response. The beams were subjected to repeated pure bending and unbending process and complete strain history was considered. The influence of axial force on the bending and springback of the elastic–ideal plastic beam was investigated by Yu and Johnson [2]. Johnson and Yu [3] developed formulas for springback of beams and plates undergoing linear work hardening. Springback of equal leg L-beams subjected to elastic–plastic pure bending was described by Xu et al. [4]. A theoretical model to predict the final geometrical configurations of wires made of different materials after loading and unloading was proposed by Baragetti [5]. Although analytical solutions can be obtained only for relatively simple problems. Their advantage is that they enable better insight and understanding of the problem and the influence of the process parameters. For more complex problems, however, the general practice is to refer to numerical techniques. Thus Li et al. [6] analyzed draw-bend tests of sheet metals using finite element modeling, where some of the results have been compared with experiments. The error associated with numerical through-thickness integration was investigated by Wagoner and Li [7]. The prediction model for springback in a wipe-bending process was developed by Kazan et al. [8] using artificial neural network approach together with the finite element method. Panthi et al. [9] analyzed and examined the effect of load on springback of a

* Corresponding author. Tel.: +386 1 4771 604; fax: +386 1 2518 567.

E-mail address: miha.brojan@fs.uni-lj.si (M. Brojan).

typical sheet metal bending process using a large deformation algorithm. Furthermore, Ragai et al. [10] investigated the influence of sheet anisotropy on the springback of drawn-bend specimens by means of experiments and finite element analysis. Vladimirov et al. [11] developed a finite strain model by combining both nonlinear isotropic and kinematic hardening, where for the integration of the equations a new algorithm based on an exponential map was used. An interesting phenomenon, a decrease of elastic modulus, can be observed in experiments on (e.g. metal) materials during plastic deformation. Ghaei [12] presented a numerical procedure which took into account also this effect. He implemented the elasto-plastic constitutive laws assuming elastic modulus as a function of effective plastic strain. The evolution of the elastic modulus with plastic deformation was also studied in other papers, see e.g. [13–20]. The change of elastic modulus during unloading is usually described by introducing the linear chord modulus [14,19,20] in many practical applications. However, experimental studies have shown that the elastic deformation during unloading is not perfectly linear. In work done by Sun and Wagoner [18] a new concept of quasi-plastic-elastic (QPE) strain was introduced within the continuum framework to model the nonlinear unloading behavior. It was shown that QPE concept is superior to the linear chord modulus in accurate prediction of springback in cases when the unloading stops at non-zero stresses.

These studies of elastic–plastic deformations of beams are mostly limited to symmetric cross-sections. Here, we present the solution procedure for elastic–plastic bending and springback of beams with asymmetric cross-sections. Elastic–nonlinear hardening behavior of the material is assumed and both isotropic and kinematic hardening models are considered. The strains are described as a function of rotation and shift of the neutral axis and the curvature of the beam. Exact geometric expressions for large deflections and large rotations are used during bending process. Strains, on the other hand, are considered to remain small. A complete loading history, including the effect of the local loading during the monotonic decrease of the load, is taken into account. Numerical examples confirm a strong influence of the load on the final and springback rotation of the neutral axis, its shift, and curvature of the beam for different cross-sections and materials. Generally, forming of beams with asymmetric cross-sections involves also torsional deformations, which we do not consider in our computations. Instead we find a special combination of forming parameters to constrain (to remove the effect of torsion from) an asymmetric rectangular L-beam to deform in one plane. Note that the presented solution procedure can easily be used for more complex shapes of cross-sections. We also present a custom-made forming tool, designed and manufactured in-house to experimentally evaluate the proposed solution procedure. Practically perfect planar shapes of the beams are obtained after forming, showing an excellent agreement with theoretical predictions, especially when the effect of the pre-strain on elastic modulus is considered.

2. Formulation of the problem

We consider a beam of asymmetric cross-section subjected to the bending moment $M(t)$ in direction α , as shown in Fig. 1, and assume an isotropic, homogeneous material which exhibits elastic–nonlinear hardening behavior. The yield point is defined by non-negative parameters σ^0 and ε^0 (cf. Fig. 3). Suppose that the beam is stress-free before loading and that the mechanical response can be described by

$$\sigma(\varepsilon; \varepsilon^0, \sigma^0) = \begin{cases} f_e(\varepsilon) & \text{for } |\varepsilon| \leq \varepsilon^0 \\ f_p(\varepsilon; \varepsilon^0, \sigma^0) & \text{for } |\varepsilon| > \varepsilon^0, \end{cases} \quad (1)$$

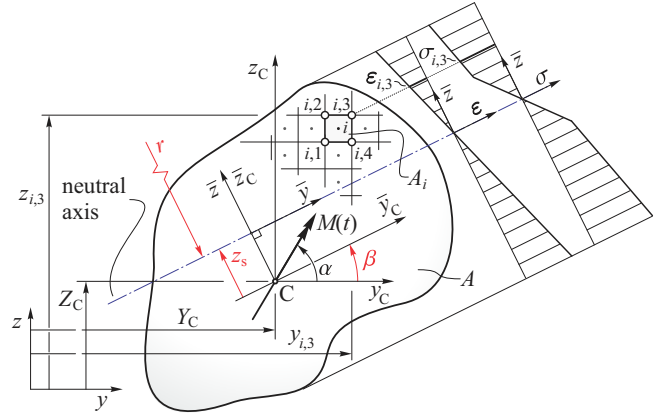


Fig. 1. Bending stress and strain state in the cross-section of the beam.

where $f_e(\varepsilon)$ and $f_p(\varepsilon; \varepsilon^0, \sigma^0)$ represent stress–strain response in the elastic and plastic regions, respectively. Both isotropic and kinematic hardening models are considered.

Exact geometric expressions for large deflections and large rotations are taken into account during bending process. Following the Euler–Bernoulli theory, valid for slender beams, a strain distribution over the cross-sectional area due to bending can be described by the following expression:

$$\begin{aligned} \varepsilon &= -\kappa \bar{z} \\ &= -\kappa(\bar{z}_C - z_s) \\ &= -\kappa(-(y - Y_C) \sin \beta + (z - Z_C) \cos \beta - z_s), \end{aligned} \quad (2)$$

where $\kappa = 1/r$ is the curvature of the beam (and r is its radius of curvature), β is the rotation of the neutral axis, z_s is the shift of the neutral axis from the centroid and Y_C, Z_C are the coordinates of the centerline taken from the reference coordinate system y – z (see Fig. 1). The neutral axis is found from the no-strain condition, $\varepsilon \equiv 0$. In the case of a linear elastic beam the neutral axis goes through the centroid of the cross-section.

Equations of static equilibrium of the beam $\sum_i \vec{F}_i = 0$ and $\sum_i \vec{M}_i = 0$ and static equilibrium of the infinitesimal element yield $dM_y/ds = 0$ and $dM_z/ds = 0$ (M_y, M_z are constants) in the case of pure bending, where s is a curvilinear coordinate along the length of the deformed beam (note that curvature $\kappa = d\vartheta(s)/ds$, where $\vartheta(s)$ is the angle of inclination of the plane, tangent to the beam's neutral surface, at the local coordinate s). The stress resultants are

$$N = \int_A \sigma dA, \quad M_y = - \int_A \sigma z dA, \quad M_z = \int_A \sigma y dA, \quad (3)$$

where N represents inner axial force, M_y and M_z are inner bending moments in directions of y -axis and z -axis, respectively, and σ is the normal stress. Due to the nonlinearity of the problem, the computation of integrals in Eq. (3) is numerical. The integration domain (the cross-section) is divided into n rectangular elements. A generic element A_i , $i \in \{1, 2, \dots, n\}$ (cf. Fig. 1) is defined by four nodes in which the mechanical properties are known. Since a complete loading history has to be considered and the effect of the local loading during the monotonic decrease of the bending moment occurs (and vice versa in monotonic increase of the load in non-virgin material), the bending moment $M(t) : 0 \rightarrow M_{\max}$ and $M_{\max} \rightarrow 0$ is applied incrementally, as shown in Fig. 2. Here variable t represents a pseudo-time, which is used to follow successive increments of the load (and stress and strain).

The mechanical state corresponding to the current load $M(t_0)$ thus includes a complete loading history. Since the strain in each node of the cross-section $\varepsilon_j^{t_0 - \Delta t}$, $j \in \{1, 2, \dots, n_N\}$ (where n_N is the

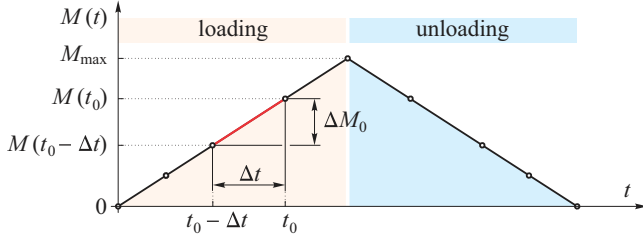


Fig. 2. Loading regime $M(t)$ and an increment of the load ΔM_0 .

total number of nodes) is known from the previous load, $M(t_0 - \Delta t)$, the change of strain in the current increment can be calculated from

$$\Delta \varepsilon_j = \varepsilon_j - \varepsilon_j^{t_0 - \Delta t}, \quad (4)$$

where strain ε_j (cf. Eq. (2)),

$$\varepsilon_j = -\kappa(-y_j - Y_C) \sin \beta + (z_j - Z_C) \cos \beta - z_s, \quad (5)$$

is a function of three variables, κ , β and z_s . Note that we write ε_j instead of $\varepsilon_j^{t_0}$ for the strain in the current increment.

Using an algorithm for updating the stress–strain relations, presented in Section 2.1 and Appendix B, the change of the stress can be calculated for each node of the cross-section:

$$\Delta \sigma_j = \sigma_j^{\text{up}}(\Delta \varepsilon_j), \quad (6)$$

$j \in \{1, 2, \dots, n_N\}$. Unknown κ , β and z_s (Eq. (5)) are computed numerically from

$$\begin{aligned} \Delta N &= \int_A \Delta \sigma \, dA \rightarrow 0 = \frac{1}{4} \sum_{i=1}^n \sum_{k=1}^4 \Delta \sigma_{i,k} A_i, \\ \Delta M_y &= - \int_A \Delta \sigma z \, dA \rightarrow \Delta M_0 \cos \alpha = \frac{1}{4} \sum_{i=1}^n \sum_{k=1}^4 \Delta \sigma_{i,k} z_{i,k} A_i, \\ \Delta M_z &= \int_A \Delta \sigma y \, dA \rightarrow \Delta M_0 \sin \alpha = -\frac{1}{4} \sum_{i=1}^n \sum_{k=1}^4 \Delta \sigma_{i,k} y_{i,k} A_i. \end{aligned} \quad (7)$$

Quasi-Newton iterative method and trapezoidal integration rule are used [22].

Finally, the current stress can be calculated as

$$\sigma_j = \sigma_j^{t_0 - \Delta t} + \Delta \sigma_j, \quad (8)$$

where $\sigma_j^{t_0 - \Delta t}$ represents the stress known from the previous increment.

2.1. Algorithm for updating stress–strain relations

In this subsection, a computational procedure is presented for updating the stress–strain relations of the j -th fiber. The isotropic hardening model is considered. Based on diagrams in Fig. 3, updated $\sigma_j^{\text{up}}(\varepsilon_j^{\text{up}})$, which are used to find the change of the stress $\Delta \sigma_j$ between the current and previous load, can be described by the modified stress–strain relation of the virgin material $\sigma_j^{\text{mod}}(\varepsilon_j^{\text{mod}})$ shifted by the stress σ_j^s and strain ε_j^s according to the $\sigma_j^{\text{up}} - \varepsilon_j^{\text{up}}$ coordinate system. This can be written as

$$\sigma_j^{\text{up}}(\varepsilon_j^{\text{up}}) = \sigma_j^{\text{mod}}(\varepsilon_j^{\text{up}} - \varepsilon_j^s) + \sigma_j^s, \quad (9)$$

$$\sigma_j^{\text{mod}}(\varepsilon_j^{\text{mod}}) = \sigma_j(\varepsilon_j^{\text{mod}}; \varepsilon_j^{0, \text{up}}, \sigma_j^{0, \text{up}}, \varepsilon_j^{\text{fp}}, \sigma_j^{\text{fp}}), \quad (10)$$

$$\sigma_j(\varepsilon_j^{\text{mod}}; \varepsilon_j^{0, \text{up}}, \sigma_j^{0, \text{up}}, \varepsilon_j^{\text{fp}}, \sigma_j^{\text{fp}}) = \begin{cases} f_e(\varepsilon_j^{\text{mod}}) & \text{for } |\varepsilon_j^{\text{mod}}| \leq \varepsilon_j^{0, \text{up}} \\ f_p(\varepsilon_j^{\text{mod}}; \varepsilon_j^{0, \text{up}}, \sigma_j^{0, \text{up}}, \varepsilon_j^{\text{fp}}, \sigma_j^{\text{fp}}) & \text{for } |\varepsilon_j^{\text{mod}}| > \varepsilon_j^{0, \text{up}}, \end{cases} \quad (11)$$

where an updated yield point is defined by $\sigma_j^{0, \text{up}}$ and $\varepsilon_j^{0, \text{up}}$. With the two additional (non-negative) parameters σ_j^{fp} and $\varepsilon_j^{\text{fp}}$ (due to the change of the plastic stress–strain response in the complete loading history), Eq. (11) represents the modified stress–strain relation of the virgin material (defined by Eq. (1)).

Linear function f_e , from Eq. (11), describes the stress–strain relation in elastic region ($|\varepsilon_j^{\text{mod}}| \leq \varepsilon_j^{0, \text{up}}$),

$$f_e(\varepsilon_j^{\text{mod}}) = \text{sign}(\varepsilon_j^{\text{mod}}) |\varepsilon_j^{\text{mod}}| E, \quad (12)$$

where E represents the modulus of elasticity. The plastic response is described by f_p , valid in $|\varepsilon_j^{\text{mod}}| > \varepsilon_j^{0, \text{up}}$. For the purposes of our study we choose the modified Ludwick law with three material parameters E_L , k_L and ε_L (see [21,23,24] for details):

$$\begin{aligned} f_p(\varepsilon_j^{\text{mod}}; \varepsilon_j^{0, \text{up}}, \sigma_j^{0, \text{up}}, \varepsilon_j^{\text{fp}}, \sigma_j^{\text{fp}}) &= \text{sign}(\varepsilon_j^{\text{mod}}) \\ &\times \left[\sigma_j^{0, \text{up}} - \sigma_j^{\text{fp}} + E_L \left(\left[|\varepsilon_j^{\text{mod}}| + \varepsilon_L - (\varepsilon_j^{0, \text{up}} - \varepsilon_j^{\text{fp}}) \right]^{1/k_L} - \varepsilon_L^{1/k_L} \right) \right]. \end{aligned} \quad (13)$$

Here, we describe the procedure for updating the stress–strain relations of the j -th fiber in each increment of the load. Isotropic hardening is considered. Graphical description is given in Fig. 3 for the first two increments of the load, where the total strain is the sum of the elastic and plastic part of the strain:

$$\varepsilon_j = \varepsilon_j^e + \varepsilon_j^p. \quad (14)$$

Pseudo-code:

1. **Start** with stored known variables for the previous load, i.e. at time $t_0 - \Delta t$: σ_j , ε_j , $\sigma_j^{0, \text{up}}$, $\varepsilon_j^{0, \text{up}}$, σ_j^{fp} , $\varepsilon_j^{\text{fp}}$, σ_j^s , ε_j^s and ε_j^p
2. An increment of the load causes change of the strain: $\Delta \varepsilon_j$
3. Calculate change of the stress state: $\Delta \sigma_j = \sigma_j^{\text{up}}(\Delta \varepsilon_j)$
4. Calculate current stress and strain state: $\sigma_j = \sigma_j + \Delta \sigma_j$; $\varepsilon_j = \varepsilon_j + \Delta \varepsilon_j$
5. Set: $\sigma_j^0 = \sigma_j^{0, \text{up}}$; $\varepsilon_j^0 = \varepsilon_j^{0, \text{up}}$
6. Check for the yield condition:
 - If $|\sigma_j| - \sigma_j^0 < 0$; Then Goto step 7
 - Else Goto step 8
7. **Elastic stress state**
 - Calculate shift of the modified stress–strain relation: $\sigma_j^s = -\sigma_j$; $\varepsilon_j^s = -(\Delta \varepsilon_j - \varepsilon_j^s)$
 - Exit
8. **Elastic–plastic stress state**
 - Update yield point: $\sigma_j^{0, \text{up}} = |\sigma_j|$; $\varepsilon_j^{0, \text{up}} = \sigma_j^{0, \text{up}} / E$
 - Calculate change of the plastic strain: $\Delta \varepsilon_j^p = |\Delta \varepsilon_j| - |\Delta \sigma_j / E|$
 - Calculate the total plastic strain: $\varepsilon_j^p = \varepsilon_j^p + \text{sign}(\Delta \varepsilon_j) \Delta \varepsilon_j^p$
 - Calculate change of the plastic response for a given increment of the load: $\Delta \sigma_j^{\text{fp}} = \sigma_j^{0, \text{up}} - \sigma_j^0$; $\Delta \varepsilon_j^{\text{fp}} = \Delta \varepsilon_j^p + \Delta \sigma_j^{\text{fp}} / E$
 - Calculate change of the plastic response over the complete loading history: $\sigma_j^{\text{fp}} = \sigma_j^{\text{fp}} + \Delta \sigma_j^{\text{fp}}$; $\varepsilon_j^{\text{fp}} = \varepsilon_j^{\text{fp}} + \Delta \varepsilon_j^{\text{fp}}$
 - Calculate shift of the modified stress–strain relation: $\sigma_j^s = -\text{sign}(\sigma_j) \sigma_j^{0, \text{up}}$; $\varepsilon_j^s = -\text{sign}(\sigma_j) \varepsilon_j^{0, \text{up}}$
 - Exit

3. Numerical examples

Based on the above procedure we present the results of numerical analysis of three examples, equal leg L-beam, T-beam and rectangular L-beam. Equilibrium (7) is satisfied within a tolerance 10^{-10} .

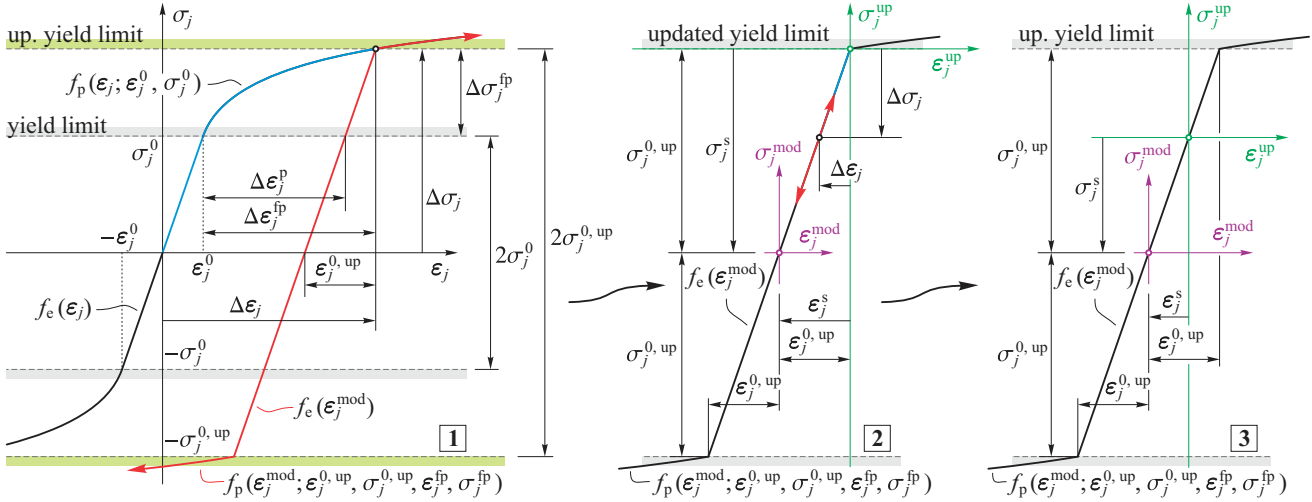


Fig. 3. Evolution of the updated stress–strain relation $\sigma_j^{up}(\epsilon_j^{up})$ of the j -th fiber, $j \in \{1, 2, \dots, n_N\}$. Isotropic hardening is considered.

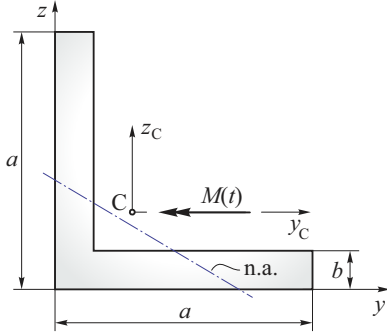


Fig. 4. Equal leg L-beam.

3.1. Equal leg L-beam

The elastic–perfectly plastic equal leg L-beam is subjected to the bending moment $M(t)$, which acts in the direction $\alpha = 180^\circ$ as shown in Fig. 4. Plastic stress–strain response is described by $f_p(\epsilon; \epsilon^0, \sigma^0) = \text{sign}(\epsilon)\sigma^0$. For the relative thickness $b/a = 0.1$ the same problem can be found in Ref. [4]. Dimensionless parameter $m = M(t)/M_e$ is introduced, where M_e represents the maximum elastic bending moment. Fig. 5 shows rotation of the neutral axis β , its shift z_s and curvature of the beam κ with respect to the parameter m for different maximum bending moments described by $m^{\max} = M_{\max}/M_e$, see Fig. 2. The complete loading–unloading process is considered and the relative thickness is fixed at $b/a = 0.1$. Relatively large differences in rotations β and shifts z_s of the neutral axis during the unloading process (when the cross-section of the beam has just been plasticized) can be observed. The effect of m^{\max} on the final rotation β^{fin} and shift z_s^{fin} of the neutral axis and the final curvature κ^{fin} of the beam for different values of the relative thickness b/a is presented in Fig. 6. The same effect on springback rotations $\beta^s = \beta^{\text{fin}} - \beta(m^{\max})$, shifts $z_s^s = z_s^{\text{fin}} - z_s(m^{\max})$ and curvatures $\kappa^s = \kappa^{\text{fin}} - \kappa(m^{\max})$ is depicted in Fig. 7.

In the case of $m^{\max} \leq 1$ (elastic region) the final shifts of the neutral axis and the final curvatures of the beam remain constant, i.e. $z_s^{\text{fin}}/a = 0.0$ and $\kappa^{\text{fin}}/\kappa_e = 0.0$, respectively, whereas the final rotations of the neutral axis also remain constant, but differ due to the relative thickness b/a , i.e. $\beta^{\text{fin}} \doteq -30.628^\circ, -30.175^\circ,$

-29.449° and -27.397° for $b/a = 0.1, 0.15, 0.2$ and 0.3 , respectively. Here, κ_e represents curvature of the beam subjected to the maximum elastic bending moment M_e .

In comparison to the results reported in [4], our calculations yield slightly different results (for the final rotation compare Fig. 6 from [4] with Fig. 6 here). We attribute the differences to the solution procedure used by [4], which included a simplified expression for rotations during the unloading process. For the case of the relative thickness $b/a = 0.2$ and maximum bending moment $m^{\max} = 1.9$ the stress states for the fully loaded and unloaded case are plotted in Fig. 8. The cross-sectional model included $n = 7600, 11,100, 14,400$ and $20,400$ square elements for $b/a = 0.1, 0.15, 0.2$ and 0.3 , respectively.

Since the stress–strain relations during the unloading differs from that in the loading process, the contours (representing the stress distribution over the cross-section) are no longer parallel to the neutral axis after unloading, see Fig. 8. It can be mentioned that rotating and shifting of the neutral axis during the unloading process causes the local loading of some fibers, especially those, which are close to the neutral axis.

3.2. T-beam

A T-beam is subjected to the bending moment $M(t)$, which acts in the direction $\alpha = -45^\circ$, as shown in Fig. 9. The material which constitutes the beam is obeying the elastic–linear hardening rheological model, as graphically described in Fig. 9. An isotropic type of strain-hardening model is considered.

The stress–strain relations of the given material can be mathematically described by the following expression:

$$\sigma(\epsilon; \epsilon^0, \sigma^0) = \begin{cases} \text{sign}(\epsilon)|\epsilon|E & \text{for } |\epsilon| \leq \epsilon^0 \\ \text{sign}(\epsilon)(\sigma^0 + E_t(|\epsilon| - \epsilon^0)) & \text{for } |\epsilon| > \epsilon^0, \end{cases} \quad (15)$$

where E_t denotes tangent modulus in the plastic region. The same as in previous numerical example, dimensionless parameter $m = M(t)/M_e$ and curvature of the beam κ_e at maximum value of the elastic bending moment M_e are employed. The relative thickness is fixed at $b/a = 2/15$.

Fig. 10 shows the relationships between the maximum bending moment and the final rotations β^{fin} , shifts z_s^{fin} and curvatures κ^{fin} for different values of the material parameter $\mu = E/E_t$. For different values of μ the influence of m^{\max} on springback rotations β^s , shifts z_s^s and curvatures κ^s are presented in Fig. 11. In Fig. 12 the

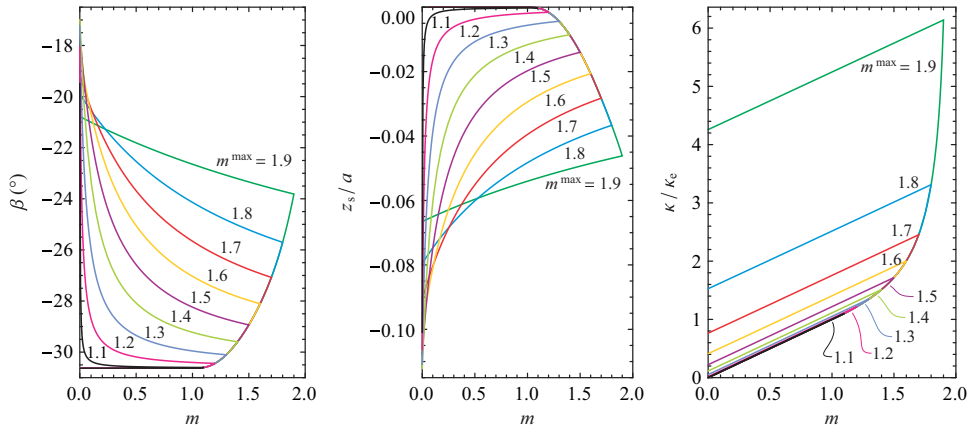


Fig. 5. Loading–unloading curves between β , z_s , κ and the bending moment for different values of m^{\max} . The relative thickness is fixed at $b/a = 0.1$.

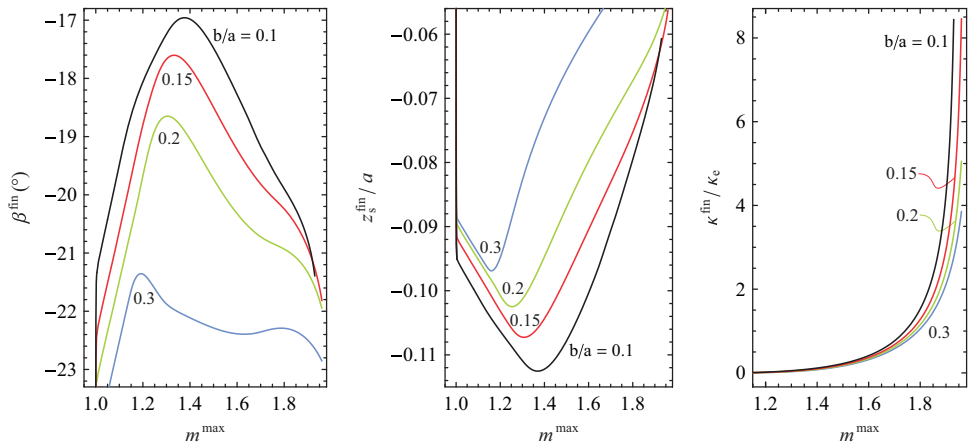


Fig. 6. Final rotations β^{fin} , shifts z_s^{fin} and curvatures κ^{fin} for different values of the relative thickness b/a .

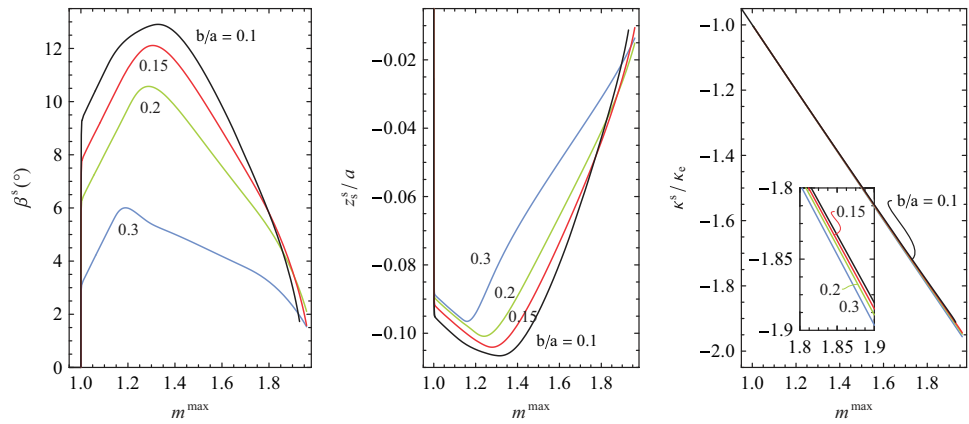


Fig. 7. Springback rotations β^s , shifts z_s^s and curvatures κ^s for different values of the relative thickness b/a .

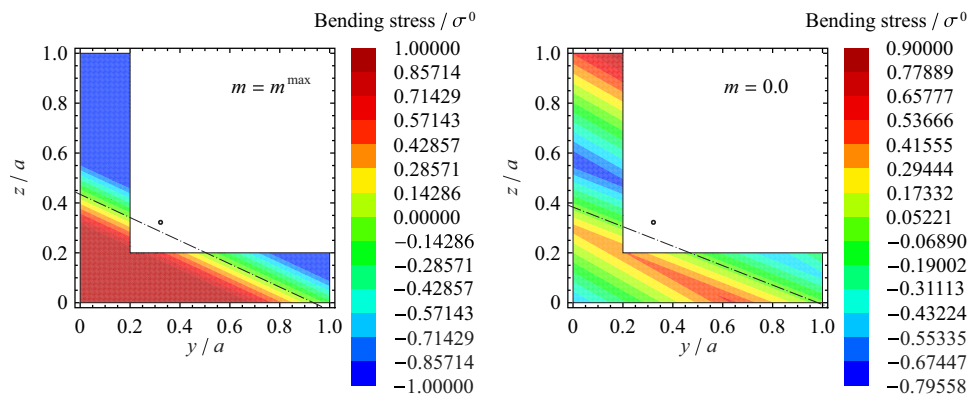


Fig. 8. Fully loaded (left) and unloaded (right) stress states for the relative thickness $b/a = 0.2$ and $m^{\max} = 1.9$.

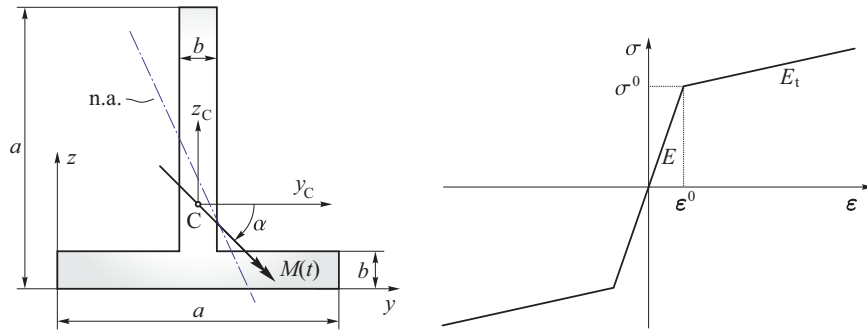


Fig. 9. T-beam (left) and the stress–strain relations of material obeying the elastic-linear hardening rheological model (right).

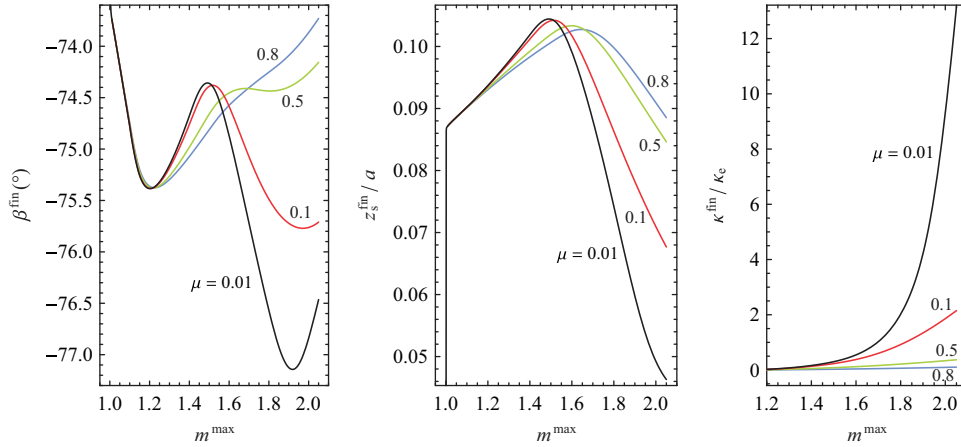


Fig. 10. Final rotations β^{fin} , shifts z_s^{fin} and curvatures κ^{fin} for different values of the material parameter μ .

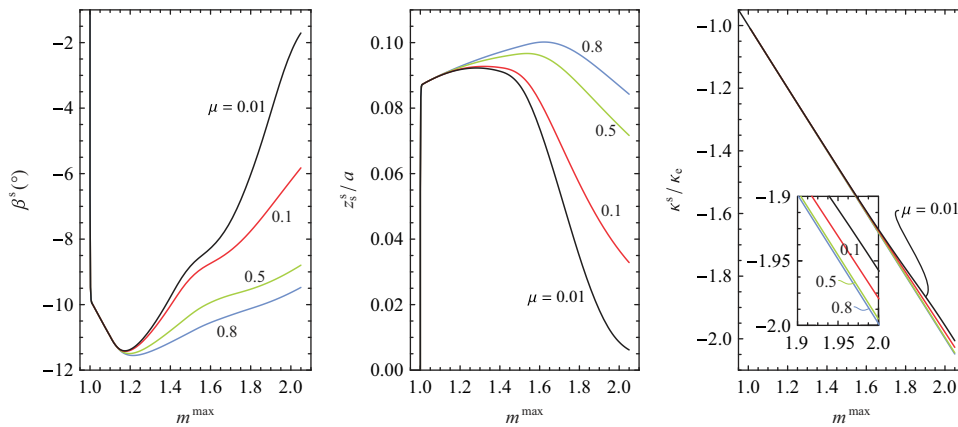


Fig. 11. Springback rotations β^s , shifts z_s^s and curvatures κ^s for different values of the material parameter μ .

effect of μ on rotations β and shifts z_s of the neutral axis and curvatures κ of the beam for the complete bending–unbending process, when the beam is subjected to the maximum bending moment $m^{\max} = 1.9$, is shown. The cross-sectional model included $n = 22,400$ square elements.

In the linear elastic case ($\mu = 1.0$) rotation and shift remain constant during the loading–unloading process, i.e. $\beta \doteq -63.778^\circ$ and $z_s/a = 0.0$, respectively, whereas curvature of the beam is proportional to the parameter m , i.e. $\kappa/\kappa_e = m$. The stress states for the fully loaded and unloaded case, with the material parameter $\mu = 0.01$ and maximum bending moment $m^{\max} = 2.0$, are plotted in Fig. 13.

Similar to the first numerical example, the contours, which represent the stresses distribution over the cross-section, are no more parallel to the neutral axis after unloading, see Fig. 13.

3.3. Rectangular L-beam

Consider a forming application (loading+unloading) where rectangular L-beam, $10 \times 15 \times 1.5$ mm in cross-section, is subjected to the bending moment $M(t)$, as shown in Fig. 14. The tool comprises a fixed circular plate of radius R with a groove at angle φ and a handle with a small wheel, which fits perfectly to the groove. As the beam is mounted to the tool at one end, the turn of the handle deforms it according to the radius of the plate. After un-mounting and springback of the beam, the final shape with radius of curvature $> R$ is obtained. We would like to find an angle φ at which a perfectly planar final shape of the beam is obtained.

The idea for solution arises from the observation of $\beta(m)$ curves (e.g. the left diagram in Fig. 5). We can assume for beams of asymmetric cross-section that during the elastic–plastic bending

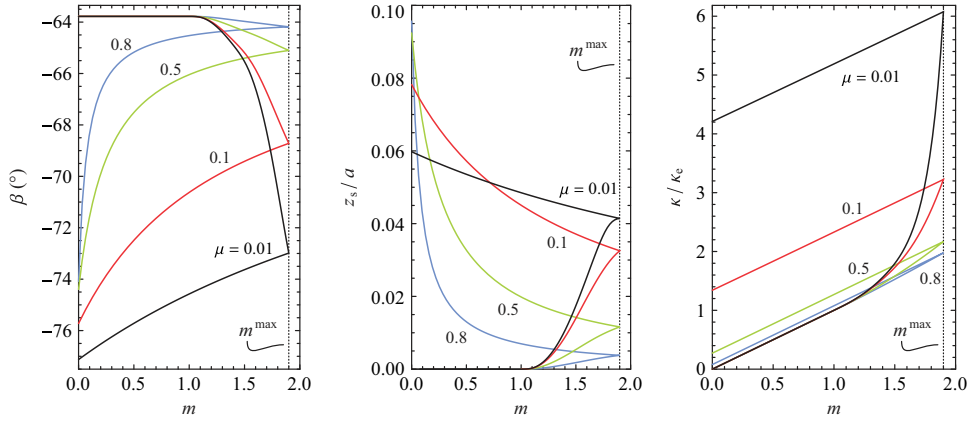


Fig. 12. Loading–unloading curves between β , z_s , κ and the bending moment for different values of the material parameter μ ($m^{\max} = 1.9$).

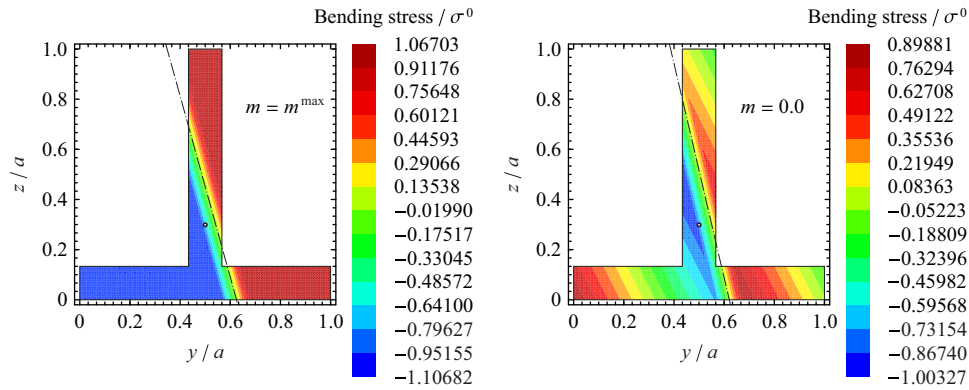


Fig. 13. Fully loaded (left) and unloaded (right) stress states for $\mu = 0.01$ and $m^{\max} = 2.0$.

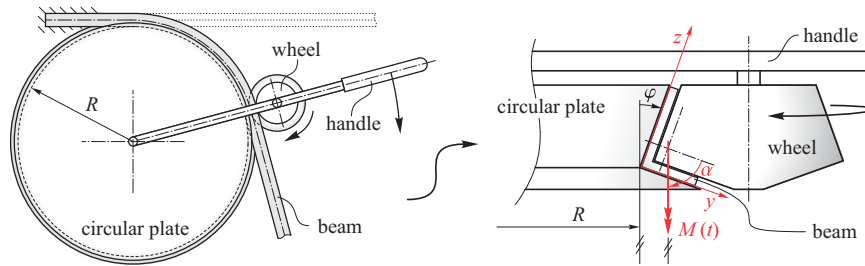


Fig. 14. Scheme of the bending tool and produced bending moment during the forming process.

process there always exists a non-zero rotation of the neutral axis β , irrespective of the (constant) direction α of the bending moment $M(t)$. The forming tool (with arbitrary φ) constrains the deformation of the beam into a plane. But according to the previous assumption, the constrained beam is also deformed in torsion. To obtain a perfectly planar shape of the beam after un-mounting, the torsional deformation would have to vanish. Let us assume further that the vanishing of the torsional deformation occurs when the mean value of rotation of the neutral axis at the beginning β_0 and that at the end of the loading process β_{\max} is equal to the direction α (the direction of the bending moment, cf. Figs. 14 and 15):

$$\alpha = \frac{\beta_0 + \beta_{\max}}{2} \tag{16}$$

Here the rotation of the neutral axis β_{\max} is the rotation β at the maximum bending moment M_{\max} , which is determined from the predefined radius of the circular plate R , rotation $\beta(M_{\max})$, shift of

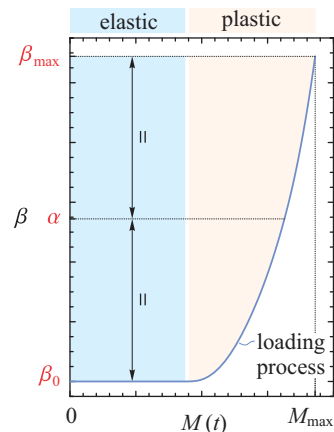


Fig. 15. Vanishing of the torsional deformations during the loading process.

the neutral axis $z_s(M_{\max})$ and curvature of the beam $\kappa(M_{\max})$, Fig. 16. According to M_{\max} , the following expression has to be satisfied:

$$R = r^P = r - \bar{z}^P = r - (\bar{z}_C^P - z_s). \quad (17)$$

Angle φ can be found in four steps:

1. Assume the direction α of the bending moment (see Fig. 14).
2. Determine the maximum bending moment M_{\max} to satisfy the condition (17).

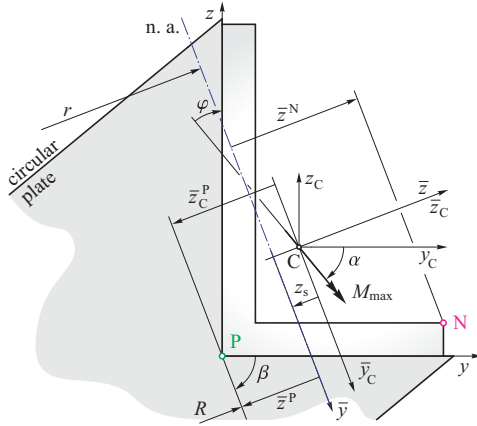


Fig. 16. Maximum bending moment M_{\max} which causes a given fiber of the cross-section (e.g. fiber P) to take a predefined radius of curvature R.

3. Check the condition for vanishing of the torsional deformations, Eq. (16). If the condition is satisfied, search for α is finished, otherwise go to step 1.
4. Calculate φ from $-\alpha + \varphi = 90^\circ$ (see Figs. 14 and 16).

If we consider material parameters of aluminum alloy 6060 T6 (material properties are listed in Appendix A), the following results are obtained: $\alpha = -70.62444^\circ$, $\varphi = 19.37556^\circ$, $M_{\max} = 12,159.14021$ N mm, $\beta_0 = -67.20665^\circ$, $\beta_{\max} = -74.04224^\circ$, $z_s(M_{\max}) = -0.38904$ mm, $\kappa(M_{\max}) = -9.66542 \times 10^{-3}$ mm $^{-1}$ \rightarrow $r(M_{\max}) = -103.46160$ mm, $r^P(M_{\max}) = -100.0$ mm, $z_s^{\text{fin}} = -0.43965$ mm, $\kappa^{\text{fin}} = -8.57985 \times 10^{-3}$ mm $^{-1}$ \rightarrow $r^{\text{fin}} = -116.55215$ mm, $r^{P,\text{fin}} = -113.20583$ mm. Note that the cross-section is modeled by $n=14,100$ square elements of dimensions 0.05×0.05 mm. Radius of the plate is $R = 100.0$ mm, which means that according to the presented formulation the radius of curvature of the circular plate is -100.0 mm. Note that maximum strain did not exceed $\varepsilon = 0.06346$ (fiber N, Fig. 16).

Fig. 17 shows rotations β and shifts z_s of the neutral axis and curvatures κ of the beam for the complete loading–unloading process. The stress and strain states for the fully loaded case are plotted in Fig. 18, whereas the stress state after unloading is shown in Fig. 19. Contrary to the stress distribution, the contours representing the strain distribution over the cross-section are always parallel to the neutral axis, Eq. (2).

In the case of kinematic hardening model, which is presented in Appendix B, the final radius of curvature of fiber P is $r^{P,\text{fin}} = -113.22151$ mm. Obviously strain path reversal can be found in some fibers. The relative difference between results obtained by both hardening models is only -0.01385% .

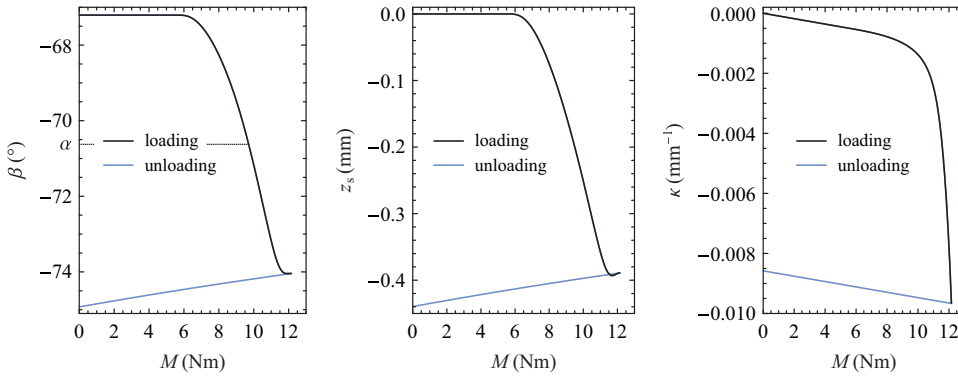


Fig. 17. Loading–unloading curves between β , z_s , κ and the bending moment.

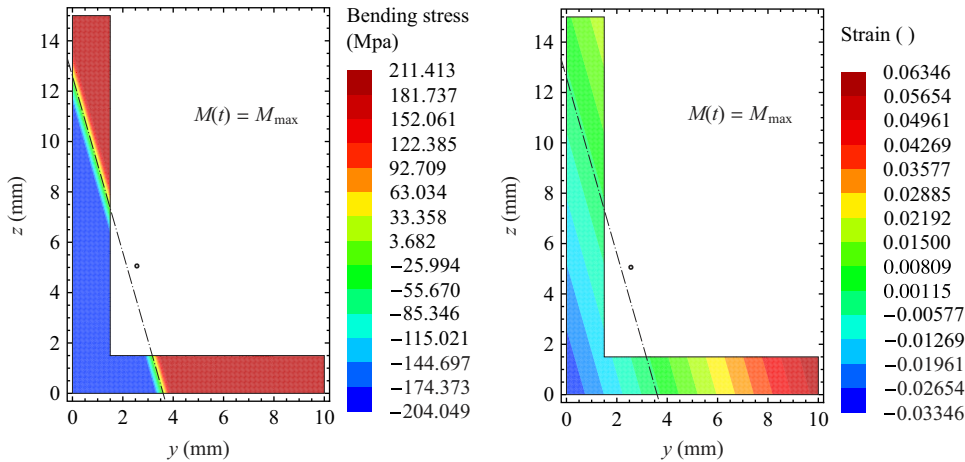


Fig. 18. Fully loaded stress (left) and strain (right) states.

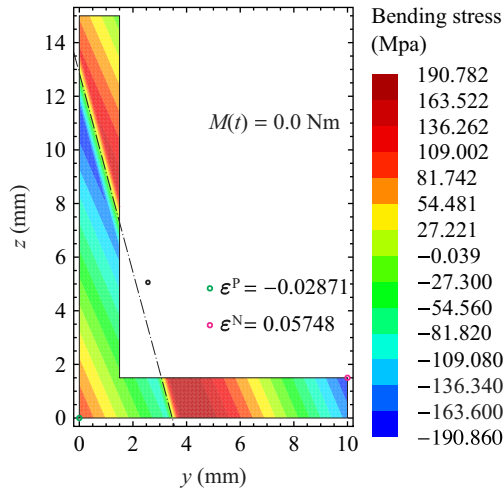


Fig. 19. The stress state after unloading. Strains in P and N.



Fig. 20. Custom-made forming tool.



Fig. 21. Plane deformation state of the formed beam (for angle $\varphi = 19.38^\circ$).

4. Experiment

A custom-made forming tool was designed and manufactured in-house to experimentally evaluate the proposed solution procedure and results obtained in numerical example 3.3. The schematics and its practical realization are shown in Figs. 14 and 20.

Note that, in general, this forming tool does not enable only pure bending conditions. But, for this particular purpose (for a carefully prescribed φ), it enables the same final deformations of the beam as obtained from pure bending – the result is a circular arch. The circular plate of radius $R = 100$ mm with a groove at angle $\varphi = 19.38^\circ$ was used.

We performed experiments on 10 specimens, rectangular L-beams ($10 \times 15 \times 1.5$ mm in cross-section and $L = 500$ mm in length) made of aluminum alloy 6060 T6. After the forming

process, the beams take a shape of a circular arch (essentially flat) as shown in Fig. 21. Just for illustration, a photo is shown in Fig. 22 of spatial deformation of the beam caused by additional torsion which originated from the incorrect angle of the groove $\varphi = 23.55^\circ$.

For each formed beam the final radius of curvature of fiber P was measured (see Fig. 16). The relative differences ϵ_r between theoretically ($r^{P,fin} = -113.20583$ mm) and experimentally determined final radii of curvature of fiber P can be found in Table 1, where the average relative difference is $-2.217 \pm 0.699\%$ (the uncertainty is the s.d. of the mean).

4.1. The effect of pre-strain on elastic modulus

In the present formulation and numerical examples it is assumed that the elastic modulus remains constant during the loading–unloading process. From additional experimental tests on cyclic loading of our aluminum specimens we observe an effect of pre-strain on elastic modulus (see Figs. 23, 24 and Table 2).

The evolution of the elastic modulus can be described with a scalar function of change of the plastic strain response over the complete loading history ϵ^{fp} using a saturated type function which has been widely used for metallic materials [12,14,19,20]. Following the formalism from the literature, we model the elastic modulus as

$$E(\epsilon^{fp}) = E_0 - (E_0 - E_{sat})(1 - e^{-\xi \epsilon^{fp}}), \quad (18)$$

where E_{sat} and ξ are two material parameters, E_{sat} is the saturated elastic modulus and E_0 is the initial elastic modulus. The initial value of elastic modulus of aluminum alloy 6060 T6 is $E_0 = 67322.455$ MPa. By fitting the measured elastic modulus during the unloading and using Eq. (18), we found $E_{sat} = 49,807.318$ MPa and $\xi = 34.374$. In Fig. 24, we show values of the elastic modulus (during unloading) from measurements and diagram of a fitting function at different pre-strains. It can be seen that the elastic

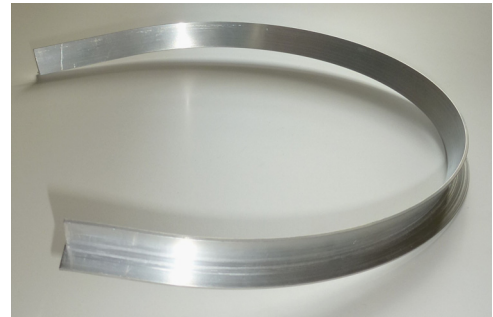


Fig. 22. Spatial deformation state of the formed beam (for angle $\varphi = 23.55^\circ$).

Table 1

The comparison between theoretically and experimentally determined final radii of curvature of fiber P.

#	$r_{exp}^{P,fin}$ (mm)	ϵ_r (%)
1	-116.105	-2.561
2	-114.982	-1.569
3	-114.464	-1.111
4	-115.980	-2.451
5	-115.427	-1.962
6	-114.934	-1.527
7	-117.146	-3.481
8	-115.319	-1.867
9	-116.167	-2.616
10	-116.630	-3.025
Aver.	-115.715	-2.217

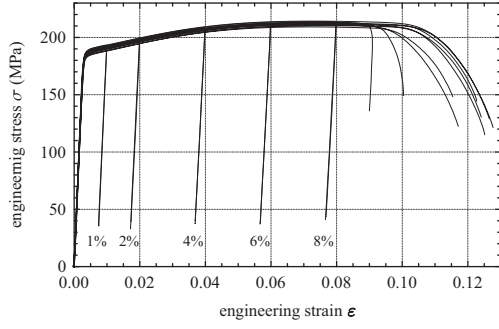


Fig. 23. Experimental stress–strain curves of cyclic loading of the specimens made of aluminum alloy 6060 T6 for five different pre-strains.

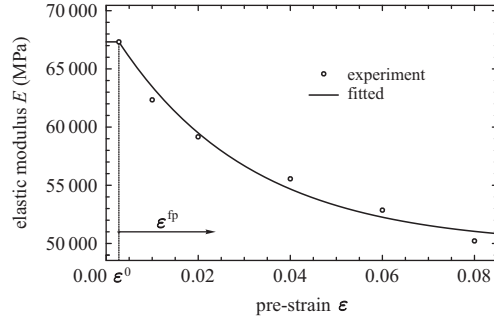


Fig. 24. Elastic modulus as a function of pre-strain.

Table 2

The effect of pre-strain on elastic modulus. The linear chord modulus model was adopted.

#	ϵ (%)	E (MPa)
1	$\epsilon^0 = 0.2766$	67,322.455
2	1.0	62,343.272
3	2.0	59,158.412
4	4.0	55,556.024
5	6.0	52,865.855
6	8.0	50,219.493

modulus rapidly decreases and saturates to E_{sat} as the pre-strain increases.

This effect can easily be implemented in algorithm for updating stress–strain relations presented in Section 2.1, where the stress–strain relation in the elastic region f_e , Eq. (12), is now written as

$$f_e(\epsilon_j^{\text{mod}}) = \text{sign}(\epsilon_j^{\text{mod}}) \epsilon_j^{\text{mod}} |E_j|, \quad (19)$$

for $j \in \{1, 2, \dots, n_N\}$, and some changes in steps 7 and 8 of the pseudo-code are implemented, i.e.

7. Elastic stress state

- Calculate shift of the modified stress–strain relation: $\sigma_j^s = -\sigma_j$; $\epsilon_j^s = -(\Delta\epsilon_j - \epsilon_j^s)$
- Calculate the total plastic strain: $\epsilon_j^p = \epsilon_j^p + \text{sign}(\Delta\epsilon_j) (|\Delta\epsilon_j| - |\Delta\sigma_j/E(0)|)$
- **Exit**

8. Elastic–plastic stress state

- Update yield stress: $\sigma_j^{0, \text{up}} = |\sigma_j|$
- Calculate change of the plastic strain: $\Delta\epsilon_j^p = |\Delta\epsilon_j| - |\Delta\sigma_j/E(0)|$
- Calculate the total plastic strain: $\epsilon_j^p = \epsilon_j^p + \text{sign}(\Delta\epsilon_j) \Delta\epsilon_j^p$

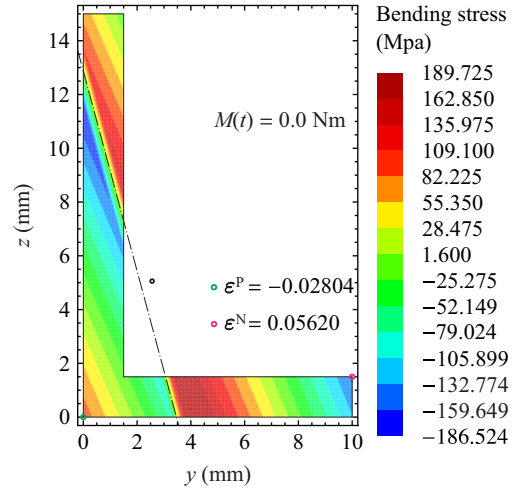


Fig. 25. The stress state after unloading. The effect of pre-strain on elastic modulus is taken into consideration. Strains in P and N.

- Calculate change of the plastic response for a given increment of the load: $\Delta\sigma_j^p = \sigma_j^{0, \text{up}} - \sigma_j^0$; $\Delta\epsilon_j^p = |\Delta\epsilon_j| - |\Delta\sigma_j/E_j| + \Delta\sigma_j^p/E_j$
- Calculate change of the plastic response over the complete loading history: $\sigma_j^{\text{fp}} = \sigma_j^p + \Delta\sigma_j^p$; $\epsilon_j^{\text{fp}} = \epsilon_j^p + \Delta\epsilon_j^p$
- Update elastic modulus: $E_j = E(\epsilon_j^{\text{fp}})$
- Update yield strain: $\epsilon_j^{0, \text{up}} = \sigma_j^{0, \text{up}}/E_j$
- Calculate shift of the modified stress–strain relation: $\sigma_j^s = -\text{sign}(\sigma_j) \sigma_j^{0, \text{up}}$; $\epsilon_j^s = -\text{sign}(\sigma_j) \epsilon_j^{0, \text{up}}$
- **Exit**

Finally, if the effect of pre-strain on elastic modulus is taken into consideration and if the beam is curved along the circular plate of radius $R = 100.0$ mm as in numerical example 3.3, the following results are obtained: $z^{\text{fin}} = -0.44116$ mm, $\kappa^{\text{fin}} = -8.38478 \times 10^{-3}$ mm $^{-1} \rightarrow r^{\text{fin}} = -119.26376$ mm, $r^{\text{P,fin}} = -115.92016$ mm. The stress state after the unloading process is plotted in Fig. 25. In comparison to the results of the final radii of curvature of fiber P determined by experiments, Table 1, the average relative difference $\epsilon_r = 0.177 \pm 0.683\%$ is obtained.

As expected, the stresses in Fig. 25 are lower in comparison to the stresses in Fig. 19, where the effect of pre-strain on elastic modulus is not considered. By decreasing of the elastic modulus the formed beam exhibits more springback, i.e. $r^{\text{P,s}} = r^{\text{P,fin}} - r^{\text{P}}(M_{\text{max}}) = -15.92016$ mm (in the case of $E = \text{const.}$, $r^{\text{P,s}} = -13.20583$ mm).

5. Conclusion

We analyzed the problem of elastic–plastic bending and springback of beams of asymmetric cross-section. We introduced a procedure for numerical computation of stress and strain states of this geometric and material nonlinear problem. A complete loading history was taken into account including the effect of the local loading during the monotonic decrease of the load. The strains are described as a function of rotation and shift of the neutral axis and the curvature of the beam. The presented algorithm involves a scheme for updating stress–strain relations of each fiber of the cross-section, and is used to calculate the change of the stress for each increment of the load. Numerical examples confirm a strong influence of maximum bending moment on the final and springback rotation of the neutral axis, its shift, and curvature of the beam for different cross-sections and materials. Both isotropic and kinematic strain-hardening models are

considered. It was shown that for the chosen example the relative difference between results obtained by both hardening models is practically negligible, but not zero (the results lie within 0.01385%). Note that our solution procedure can be used for arbitrary loading regime (such as multi-cycle and non-monotonic loading) and also more complex materials (composite, functionally graded, etc.).

A custom-made forming tool was designed and manufactured in-house to experimentally evaluate the proposed solution procedure. A rectangular L-beam made of an aluminum alloy 6060 T6 was used and its material properties were carefully measured. The first task in this example was to determine an appropriate angle φ of the groove on circular plate at which a perfectly planar final shape of the beam would be obtained after forming (to remove the effect of torsion). It was shown that relative difference between theoretically predicted and experimental measurements of the final radius of curvature of the formed beam was

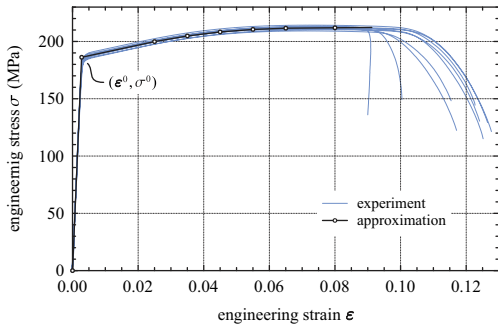


Fig. 26. Experimental and approximated stress–strain curves of aluminum alloy 6060 T6.

Table 3
Approximated stress–strain curve of aluminum alloy 6060 T6.

#	σ (MPa)	ϵ ()	E_t (MPa)
1	0.000	0.000	
2	$\sigma^0 = 186.187$	$\epsilon^0 = 2.766 \times 10^{-3}$	$E = 67,322.455$
3	199.881	0.025	615.910
4	204.809	0.035	492.728
5	208.319	0.045	351.069
6	210.475	0.055	215.568
7	211.584	0.065	110.864
8	211.953	0.080	24.636

within $-2,217 \pm 0,699\%$, if the elastic modulus was considered to remain constant during the deformation. Including an additional feature, the effect of pre-strain on elastic modulus (evolution of the elastic modulus), in our algorithm, enabled a better description of a real material behavior. We obtained an excellent agreement with experiments. The results differed from experiments by only $\epsilon_r = 0.177 \pm 0.683\%$ in average.

Appendix A. Measuring mechanical properties of aluminum alloy 6060 T6

Material properties were measured on a Zwick Z050 measuring device, equipped with Multisens extensometers. The measured stress–strain curves of nine flat specimens (cut from the $10 \times 15 \times 1.5$ mm L-beams) are illustrated in Fig. 26. Nine tests (one had to be discarded due to the technical difficulties) were performed at the same experimental conditions (cross-head speed=10 mm/min, cross-head travel resolution=40.0 μ m and temperature=20 $^\circ$ C) and then piecewise approximated by seven linear functions, as shown in Fig. 26 and given Table 3.

Note that E_t is approximated to be constant after 0.08 of strain, i.e. $E_t = 24.636$ MPa for $\epsilon > 0.08$.

Appendix B. Algorithm for updating stress–strain relations when the kinematic hardening model is taken into consideration

A computational procedure for updating stress strain relations $\sigma_j^{up}(\epsilon_j^{up})$ of j -th fiber of the cross-section prepared for the next increment of the load, when the kinematic hardening model is taken into consideration, can be expressed in the way very similar to the isotropic hardening model, see Fig. 27. Updated stress–strain relation $\sigma_j^{up}(\epsilon_j^{up})$ can be described by Eqs. (9), (10) and (11) and (11), where the yield point, expressed by σ_j^0 and ϵ_j^0 , is constant for the complete loading–unloading process.

Additional parameter σ_j^{syl} is involved and represents a shift of the upper and lower yield limits according to σ_j - ϵ_j coordinate system. Here, we describe the procedure for updating the stress–strain relations of j -th fiber in each increment of the load. Graphical description is given in Fig. 27 for the first increment of the load.

Pseudo-code.

1. **Start** with stored known variables for the previous load, i.e. at time $t_0 - \Delta t$: $\sigma_j, \epsilon_j, \sigma_j^{fp}, \epsilon_j^{fp}, \sigma_j^s, \epsilon_j^s, \epsilon_j^p$ and σ_j^{syl}
2. An increment of the load causes change of the strain: $\Delta \epsilon_j$

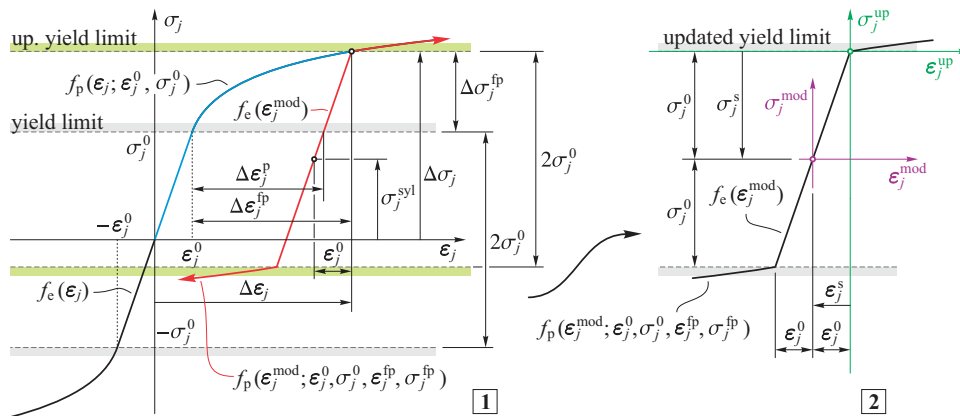


Fig. 27. Evolution of the updated stress–strain relation $\sigma_j^{up}(\epsilon_j^{up})$ of the j -th fiber, $j \in \{1, 2, \dots, n_N\}$. Kinematic hardening is considered.

3. Calculate change of the stress state: $\Delta\sigma_j = \sigma_j^{\text{up}}(\Delta\varepsilon_j)$
4. Calculate current stress and strain state: $\sigma_j = \sigma_j + \Delta\sigma_j$;
 $\varepsilon_j = \varepsilon_j + \Delta\varepsilon_j$
5. Check for the yield condition:
 - **If** $|\sigma_j - \sigma_j^{\text{sy}}| - \sigma_j^0 < 0$; **Then Goto** step 6
 - **Else Goto** step 7
6. **Elastic stress state**
 - Calculate shift of the modified stress–strain relation:
 $\sigma_j^s = -(\sigma_j - \sigma_j^{\text{sy}})$; $\varepsilon_j^s = -(\Delta\varepsilon_j - \varepsilon_j^s)$
 - **Exit**
7. **Elastic–plastic stress state**
 - Calculate change of the plastic strain: $\Delta\varepsilon_j^{\text{p}} = |\Delta\varepsilon_j| - |\Delta\sigma_j/E|$
 - Calculate the total plastic strain: $\varepsilon_j^{\text{p}} = \varepsilon_j^{\text{p}} + \text{sign}(\Delta\varepsilon_j)\Delta\varepsilon_j^{\text{p}}$
 - Calculate change of the plastic response for a given increment of the load:
 - **If** $\Delta\sigma_j = 0$; **Then** $\Delta\sigma_j^{\text{fp}} = 0$
 - **Else** $\Delta\sigma_j^{\text{fp}} = |\Delta\sigma_j| - \sigma_j^0 - \text{sign}(\Delta\sigma_j)\sigma_j^s$
 - $\Delta\varepsilon_j^{\text{fp}} = \Delta\varepsilon_j^{\text{p}} + \Delta\sigma_j^{\text{fp}}/E$
 - Calculate change of the plastic response over the complete loading history: $\sigma_j^{\text{fp}} = \sigma_j^{\text{fp}} + \Delta\sigma_j^{\text{fp}}$; $\varepsilon_j^{\text{fp}} = \varepsilon_j^{\text{fp}} + \Delta\varepsilon_j^{\text{fp}}$
 - Calculate shift of the modified stress–strain relation:
 $\sigma_j^s = -\text{sign}(\sigma_j - \sigma_j^{\text{sy}})\sigma_j^0$; $\varepsilon_j^s = -\text{sign}(\sigma_j - \sigma_j^{\text{sy}})\varepsilon_j^0$
 - Calculate shift of the yield limits:
 - **If** $\Delta\sigma_j = 0$; **Then** $\sigma_j^{\text{sy}} = \sigma_j^{\text{sy}}$
 - **Else** $\sigma_j^{\text{sy}} = \sigma_j - \text{sign}(\Delta\sigma_j)\sigma_j^0$
 - **Exit**

If the effect of pre-strain on elastic modulus is taken into consideration, some changes in steps 6 and 7 of the pseudo-code are implemented, i.e.

6. **Elastic stress state**
 - Calculate shift of the modified stress–strain relation:
 $\sigma_j^s = -(\sigma_j - \sigma_j^{\text{sy}})$; $\varepsilon_j^s = -(\Delta\varepsilon_j - \varepsilon_j^s)$
 - Calculate the total plastic strain: $\varepsilon_j^{\text{p}} = \varepsilon_j^{\text{p}} + \text{sign}(\Delta\varepsilon_j)(|\Delta\varepsilon_j| - |\Delta\sigma_j/E(0)|)$
 - **Exit**
7. **Elastic–plastic stress state**
 - Calculate change of the plastic strain: $\Delta\varepsilon_j^{\text{p}} = |\Delta\varepsilon_j| - |\Delta\sigma_j/E(0)|$
 - Calculate the total plastic strain: $\varepsilon_j^{\text{p}} = \varepsilon_j^{\text{p}} + \text{sign}(\Delta\varepsilon_j)\Delta\varepsilon_j^{\text{p}}$
 - Calculate change of the plastic response for a given increment of the load:
 - **If** $\Delta\sigma_j = 0$; **Then** $\Delta\sigma_j^{\text{fp}} = 0$
 - **Else** $\Delta\sigma_j^{\text{fp}} = |\Delta\sigma_j| - \sigma_j^0 - \text{sign}(\Delta\sigma_j)\sigma_j^s$
 - $\Delta\varepsilon_j^{\text{fp}} = |\Delta\varepsilon_j| - |\Delta\sigma_j/E_j| + \Delta\sigma_j^{\text{fp}}/E_j$
 - Calculate change of the plastic response over the complete loading history: $\sigma_j^{\text{fp}} = \sigma_j^{\text{fp}} + \Delta\sigma_j^{\text{fp}}$; $\varepsilon_j^{\text{fp}} = \varepsilon_j^{\text{fp}} + \Delta\varepsilon_j^{\text{fp}}$
 - Update elastic modulus: $E_j = E(\varepsilon_j^{\text{fp}})$
 - Update yield strain: $\varepsilon_j^0 = \sigma_j^0/E_j$
 - Calculate shift of the modified stress–strain relation:
 $\sigma_j^s = -\text{sign}(\sigma_j - \sigma_j^{\text{sy}})\sigma_j^0$; $\varepsilon_j^s = -\text{sign}(\sigma_j - \sigma_j^{\text{sy}})\varepsilon_j^0$

- Calculate shift of the yield limits:
 - **If** $\Delta\sigma_j = 0$; **Then** $\sigma_j^{\text{sy}} = \sigma_j^{\text{sy}}$
 - **Else** $\sigma_j^{\text{sy}} = \sigma_j - \text{sign}(\Delta\sigma_j)\sigma_j^0$
- **Exit**

References

- [1] Kosel F, Videnic T, Kosel T, Brojan M. Elasto-plastic springback of beams subjected to repeated bending/unbending histories. *J Mater Eng Perform* 2011;20:846–54.
- [2] Yu TX, Johnson W. Influence of axial force on the elastic–plastic bending and springback of a beam. *J Mech Work Technol* 1982;6:5–21.
- [3] Johnson W, Yu TX. On springback after the pure bending of beams and plates of elastic work-hardening materials III. *Int J Mech Sci* 1981;23:687–95.
- [4] Xu Y, Zhang LC, Yu TX. The elastic–plastic pure bending and springback of L-shaped beams. *Int J Mech Sci* 1987;29:425–33.
- [5] Baragetti S. A theoretical study on nonlinear bending of wires. *Meccanica* 2006;41:443–58.
- [6] Li KP, Carden WP, Wagoner RH. Simulation of springback. *Int J Mech Sci* 2002;44:103–22.
- [7] Wagoner RH, Li M. Simulation of springback: through-thickness integration. *Int J Plast* 2007;23:345–60.
- [8] Kazan R, Firat M, Tiryaki AE. Prediction of springback in wipe-bending process of sheet metal using neural network. *Mater Des* 2009;30:418–23.
- [9] Panthi SK, Ramakrishnan N, Pathak KK, Chouhan JS. An analysis of springback in sheet metal bending using finite element method (FEM). *J Mater Process Technol* 2007;186:120–4.
- [10] Ragai I, Lazim D, Nemes JA. Anisotropy and springback in draw-bending of stainless steel 410: experimental and numerical study. *J Mater Process Technol* 2005;166:116–27.
- [11] Vladimirov IN, Pietryga MP, Reese S. Prediction of springback in sheet forming by a new finite strain model with nonlinear kinematic and isotropic hardening. *J Mater Process Technol* 2009;209:4062–75.
- [12] Ghaei A. Numerical simulation of springback using an extended return mapping algorithm considering strain dependency of elastic modulus. *Int J Mech Sci* 2012;65:38–47.
- [13] Cleveland RM, Ghosh AK. Inelastic effects on springback in metals. *Int J Plast* 2002;18:769–85.
- [14] Zang S-L, Lee M-G, Kim JH. Evaluating the significance of hardening behaviour and unloading modulus under strain reversal in sheet springback prediction. *Int J Mech Sci* 2013;77:194–204.
- [15] Vin LJ, Streppl AH, Singh UP, Kals HJJ. A process model for air bending. *J Mater Process Technol* 1996;57:48–54.
- [16] Yu HY. Variation of elastic modulus during plastic deformation and its influence on springback. *Mater Des* 2009;30:846–50.
- [17] Abdel-Karim M. Effect of elastic modulus variation during plastic deformation on uniaxial and multiaxial ratchetting simulations. *Eur J Mech A/Solid* 2011;30:11–21.
- [18] Sun L, Wagoner RH. Complex unloading behavior: nature of the deformation and its consistent constitutive representation. *Int J Plast* 2011;27:1126–44.
- [19] Zang S-L, Lee M-G, Sun L, Kim JH. Measurement of the Bauschinger behavior of sheet metals by three-point bending springback test with pre-strained strips. *Int J Plast* 2014;59:84–107.
- [20] Lee J, Lee J-Y, Barlat F, Wagoner RH, Chung K, Lee M-G. Extension of quasi-plastic-elastic approach to incorporate complex plastic flow behavior—application to springback of advanced high-strength steels. *Int J Plast* 2013;45:140–59.
- [21] Brojan M, Sitar M, Kosel F. On static stability of nonlinearly elastic Euler's columns obeying the modified Ludwick's law. *Int J Struct Stab Dyn* 2012;12:1250077(1)–19.
- [22] Burden RL, Faires JD. Numerical analysis. 9th ed. Boston: Brooks/Cole; 2010.
- [23] Jung JH, Kang TJ. Large deflection analysis of fibers with nonlinear elastic properties. *Text Res J* 2005;75:715–23.
- [24] Brojan M, Videnic T, Kosel F. Large deflections of nonlinearly elastic non-prismatic cantilever beams made from materials obeying the generalized Ludwick constitutive law. *Meccanica* 2009;44:733–9.